Finite element modelling of continuous fiber–reinforced composites produced by automated manufacturing

Szederkényi B., Rácz I., Kovács N.K., Czigány T.

Accepted for publication in IOP Conference Series: Materials Science and Engineering
Published in 2024
DOI: 10.1088/1757-899X/1313/1/012002

IOP Conf. Series: Materials Science and Engineering **1313** (2024) 012002 doi:10.1088/1757-899X/1313/1/012002

Finite element modelling of continuous fiber–reinforced composites produced by automated manufacturing

B Szederkényi[1], **I Rácz**[1], **N K Kovács**[1,2] **and T Czigány**[1,3*]
[1] Department of Polymer Engineering, Faculty of Mechanical Engineering, Budapest University of Technology and Economics, Muegyetem rkp. 3., H-1111 Budapest, Hungary
[2] MTA-BME Lendület Lightweight Polymer Composites Research Group, Muegyetem rkp. 3., H-1111 Budapest, Hungary
[3] HUN-REN-BME Research Group for Composite Science and Technology, Muegyetem rkp. 3., H-1111 Budapest, Hungary
* corresponding author: czigany@eik.bme.hu

Abstract. With the advent of automated, continuous filament placement technologies, the possibilities for reinforcement placement in composite manufacturing have been further expanded, as the reinforcement path can be continuously varied within the layer. This allows far more efficient structures to be created, resulting in a further reduction in the weight of the structure compared to conventional composites. At the same time, this manufacturing freedom also poses a major challenge for the structural design of composite components, as simulation methods based on meso-level homogenization are mostly not usable due to the lack of periodicity of the reinforcement structure. In our paper, we have established a structural modelling method using finite element analysis (FEA) for fused filament fabrication-based additive manufacturing of continuous fiber–reinforced composites. For modelling the reinforcement structure properly, we used the base-coordinate sweep (BCS) modelling method and for capturing progressive failure mechanisms we used Ansys LS-Dyna with the MAT54 material card. Based on the simulations and tests performed, we demonstrated that the method we present is suitable for the engineering modelling of continuous fiber–reinforced 3D printed composites.

1. Introduction

As the world changes and evolves, engineers are increasingly driven to use and develop more resource- and energy-efficient structural elements. Achieving this goal requires the optimization and proper design of lightweight structural materials. Composites are the structural materials with the highest specific strength currently known, and to exploit their advantageous properties, it is necessary to orient the reinforcing fibers in the direction of the load. In this context, additive manufacturing has opened up new possibilities for designers. Composite 3D printing offers geometric freedom in fiber placement that would have been previously unimaginable or very difficult to achieve with conventional manufacturing technologies. However, exploiting this novel method also requires novel tools and methods to optimize complex geometries and fiber reinforcement structures. Topology Optimization (TO) satisfies this requirement, allowing engineers to find the material distribution that provides the best performance with the least material usage [1].

This paper aims to develop a procedure for structural analysis based on finite element methods (FEM) for these novel composite manufacturing technologies, including the modelling of progressive failure mechanisms.

2. Challenges in the structural analysis of composites produced by automatic fiber placement

The structural analysis of continuous fiber-reinforced 3D printed composites is a challenge in design and manufacturing due to several factors. Exploiting the intricate anisotropic properties arising from the variable orientation of the reinforcement fibers plays a key role in optimizing the components, but there is currently no widespread method for automatically incorporating these into FE models. Beyond software limitations, the situation is complicated by manufacturing specificities and current technology limitations. In the case of fused filament fabrication (FFF) based printing methods the bulk lay-up is welded in a way that it does not fill the available space due to the extruder profile [2,3]. Porosity, and interlayer welding problems during printing have a non-negligible influence on the mechanical properties of these composite parts. As porosity can exceed 10%, the failure of the part is highly dependent on the generation and propagation of micro- and meso-structural defects in porous parts under load [4]. Further difficulties are caused by the constantly evolving and therefore often changing material composition, which also requires the continuous updating of existing models to adequately model failure phenomena [5]. A key part of our work was searching for and analyzing existing material model sources and performing our validation tests. The simulation and numerical modelling of 3D printed composites is a complex, multi-level problem that requires a different approach from traditional methods.

3. Modelling of composites produced by automated fiber placement

The meso-level computational methods developed for conventional composites based on layer homogenization cannot be used for complex reinforcement structures, since the reinforcement layer cannot be described with a finite number of discrete vectors for principal directions. Instead, the mechanical behavior of composites can be more accurately described with an orientation-dependent ($\underline{M}(\theta)$) elastic matrix, where θ represents the local principal direction of reinforcement. For conventional systems, such as unidirectionally reinforced or multi-directionally reinforced fabrics with repetitive patterns, the elasticity matrix values remain constant across the whole layer. However, with automated fiber placement, these θ values could vary locally within the layer, making the structure more adaptable to specific loading conditions. This variability enhances the specific performance of the composite structure, but also eliminates traditional homogenization methods at the layer level, necessitating new modelling approaches (Figure 1: (a)). In our paper, we address this problem and present a possible solution using the base-coordinate sweep (BCS) method. The BCS procedure can consider the change of fiber orientation within the layer by treating the reinforcement bundles as the lowest level of the structure. By fitting a coordinate system running along the centerline of the fiber bundles (Figure 1: (b)), the BCS method can provide a more accurate prediction of the processes occurring in the component.

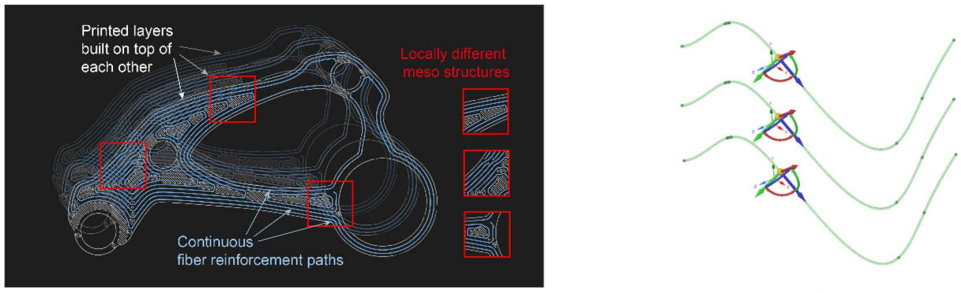

(a) (b)

Figure 1. Typical structure of composites produced with automated methods on a Formula Student car suspension part, where the meso-structure does not allow homogenization at the layer level (a) and a schematic diagram showing the base-coordinate sweep along the reinforcement curves (b)

To validate our approach, we chose a geometry from the literature [6] known to be generated by TO, thus allowing the use of complex reinforcement trajectories. Our previous paper [7] had already addressed this geometry, where we developed optimal reinforcement trajectories for the component and introduced a fiber segmentation method, which allowed us to model the stiffness of the component

correctly but did not provide any information on the post-failure process. In our current paper, we continue to work with this reinforcement structure (Figure 2).

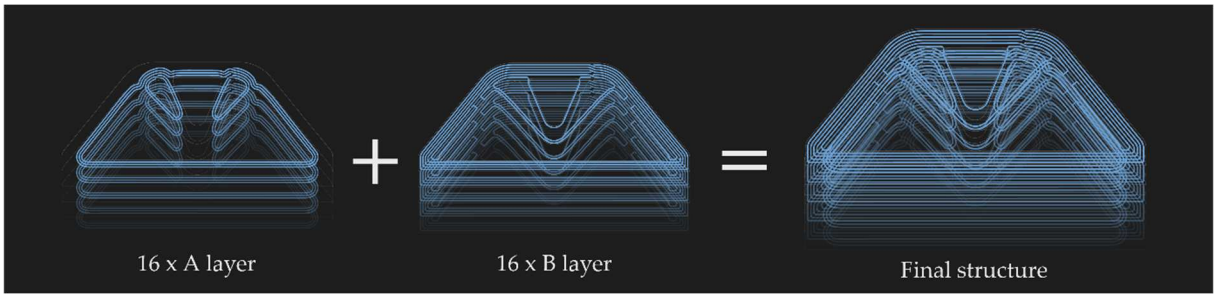

Figure 2. The final 64-layer test specimen with a reinforcement structure consisting of 2x16 alternating separate reinforcement layers and "blank" layers printed in between, containing only matrix material.

4. Manufacturing technology, materials used, material model, and the measurement environment

The composite part was 3D printed with a Markforged Mark Two FFF 3D printer, set to a layer thickness of 0.125 mm. The matrix material of the composite part was Markforged Onyx base material (PA6 filled with milled carbon fiber), the continuous filament bundle was 1K roving (1000 elementary fibers) pre-impregnated with PA6, with a fiber content of 28% and a filament diameter of 0.375 mm, taken from the literature [8,9].

For our simulations, the initial material properties of the components were taken from the literature [8,10–12], supported by our tests in the case of continuous carbon filament. However, due to the limitations of the Markforged system, which does not allow the components to be manufactured completely separated, the results obtained had to be corrected afterward to get the properties of individual components. These corrections were performed with the use of the rule of mixtures, according to Eq. (1).

$$E_f = \frac{E_{resultant} - (v_m E_m + v_v E_v)}{v_f} = 70{,}65\ [GPa] \tag{1}$$

where $\boldsymbol{E}$ is the tensile modulus of elasticity [GPa], $\boldsymbol{V}$ is the volume fraction [-], $\boldsymbol{m}$ is an index of the matrix material, $\boldsymbol{f}$ is an index of the fiber-reinforced filament, and $\boldsymbol{v}$ is an index of voids in the part, also known as the porosity of the structure. The volume fractions of the components were calculated from the cross-sectional ratios measured in our specimens and the known diameter of the fiber-reinforced filament, with simple geometric relationships.

The modulus-type and Poisson's ratio values in a non-principal direction, which cannot be determined indirectly from tensile and three-point bending tests (Figure 3. a and b), were determined with the use of the micromechanical representative volume element (RVE) modelling method, where the stiffness and principal direction strength of the filament was determined from the fiber content and Poisson's ratio of the components. Then, the shear modulus and Poisson's ratio of the continuous fiber-reinforced orthotropic UD filament (Figure 3. c) were determined by tuning the output to the measured values. Strength properties perpendicular to the principal direction, and shear strength were estimated with the values of the matrix material found in the literature [13]. The results are summarized in Table 1 (a).

The bending test was carried out on a Zwick Z250 universal testing machine, at room temperature, at a test speed of 2mm/min, on 3 specimens. We designed a fixture for the test, specifically for this non-standard specimen geometry (Figure 3 a, b). These tests were complemented by Digital Image Correlation (DIC) to track the local deformation fields of the specimen. This provided us with more accurate visual information on the progress of failure, which we later compared with the simulation.

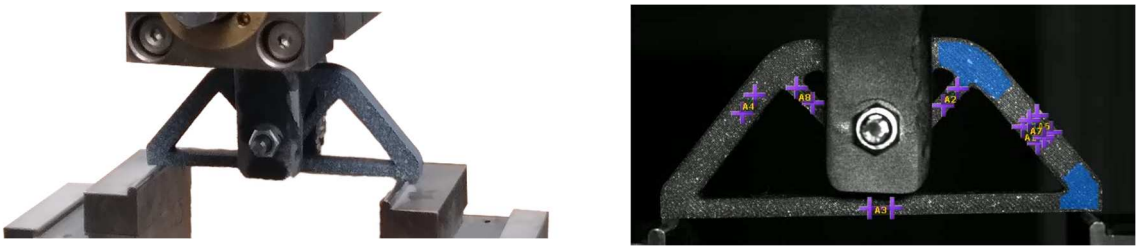

(a) (b)

Figure 3. The three-point bending arrangement of the reinforced geometry (a) and the camera image captured by the DIC system recording the exact deformations (b).

5. The simulation

5.1. CAD modelling of geometry and fiber reinforcement

For the implementation of BCS, the geometry of both the reinforcement structure and the matrix material were modelled at the micro-level, allowing tracking of the intralaminar interactions at the interfaces between the reinforcement and the matrix material. We used the simplification of merging the same layers in the construction direction (Z) of the specimen. In doing so, we sacrificed the modelling of interlaminar phenomena between the layers, but since the component was not dominated by such failure events, we did not lose any significant information by this simplification. The matrix material was modelled as a solid geometry, while the centerline of the fiber reinforcement was modelled with a surface strip of a width corresponding to the added thickness of the layers (Figure 4). Since the thickness of the printed layer is 0.125mm and filament reinforcement has a diameter of 0.375mm, the laid filament bundle can cover a width of ~0.89 mm in the XY plane.

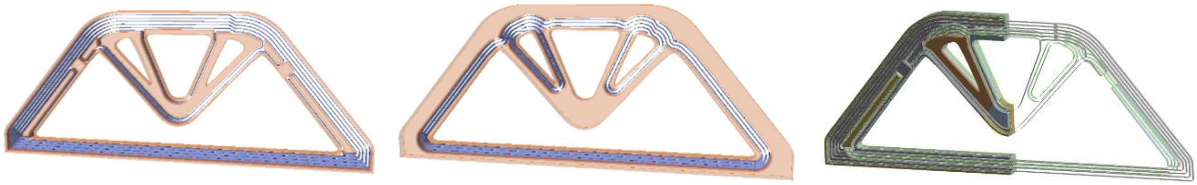

(a) (b) (c)

Figure 4. The merged geometry slices of the two applied reinforcement structures (a, b), from which the final VEM quarter model was constructed (c).

5.2. Simulation environment

The simulation was built in the Ansys Workbench 2023R2 environment. Here, we first separated the characteristic reinforcement structures (Figure 2), then solid bodies and the parts modelled as surfaces. The reinforcement structure was prepared in an ACP (Ansys Composite PrePost) environment while the matrix materials were pre-processed in the Static Structural module. Later, these modules were merged into a common Static Structural module where the final loading and contact boundary conditions were determined. Using the edges of the central surfaces representing the fiber reinforcement (Figure 5 a), we determined the trajectory in the ACP module for the implementation of BCS, on which we swept the coordinate system representing the directions of fiber reinforcement and assigned the local fiber directions to the surface elements (Figure 5). Then the central surface was symmetrically thickened according to actual fiber thickness, thus a VEM model of fiber reinforcement was created (Figure 5 c).

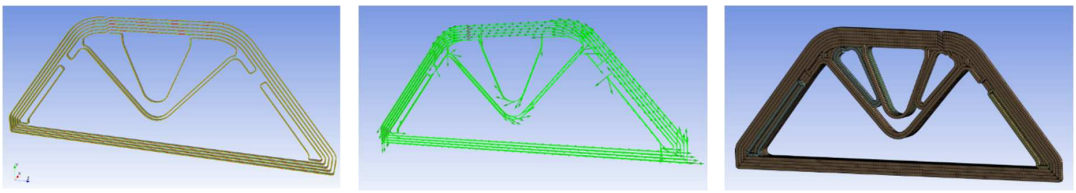

(a) (b) (c)

Figure 5. The steps of the Base Coordinate Sweep (BCS) are defining the reinforcing structure (a), performing the coordinate sweep where the green arrows indicate the direction of the fibers (b), determining the spatial extent of the reinforcing structure, and creating the finite element mesh (c).

The internal constraints of the characteristic sections (the connection of the connecting surfaces of the fiber reinforcement to themselves and the matrix) were determined in the next step, where the components were coupled by bonded constraints that are deactivated in the case of stresses above a limit value on the given surface, where shear and normal components were defined separately. With this method, separation phenomena between the printed components were modelled. The finished components were then merged into a common module, and the connections between them were also defined with a bonded constraint that terminates above the critical stress. The test specimen was defined by constraints corresponding to three-point bending with the introduction of vertical displacement through a pin passed through the center of the specimen and symmetrical support spaced at 80 mm. Both external constraints connected to the specimen with frictionless contacts.
The simulation aims to model progressive failure processes, therefore the use of explicit FEA methods is preferable, due to their ability to handle change in the substitutive properties during the calculation process far more stable, than their implicit counterparts. For that reason, we used the LS-Dyna solver integrated into Ansys Workbench.
Due to the complexity of the model and the existing symmetries, we worked with a quarter model, applying a frictionless planar constraint in the symmetry planes. We used a neglection—during printing the machine always had to cut the continuous fiber of the reinforcement structure somewhere, where reinforcement was consequently discontinuous. This is done automatically, always in a different location in the structure, and therefore the local weakening effect is always in a different place. For this reason, we simplified the reinforcement structure by assuming that it is continuous and there are no interruptions. Double symmetry can only be used with these simplifications. As a further simplification, the problem was not considered with the actual speed of load. The 5 mm crosshead displacement was applied to the system in 0.01 seconds. This was done to further reduce the computational cost of the problem. The 0.5 mm element size of the mesh and the density of the material resulted in a timestep of 4.5×10^{-5} ms, to which an adaptive mass scaling with a 1.7% increase in total mass was applied, to further reduce runtime. The mesh was constructed from linear hex8 and wed6 elements with an average quality of 0.9483±0.082 according to the built-in Ansys metric (1 being the maximum, at which point the mesh is perfect). With these settings, the simulation runtime at full processor use was ~2 hours per iteration on an Intel I7-7700K, 4.2 GHz processor with 4 cores and 8 logic threads.

5.3. *The applied simulation material model*

The MAT54 material card, also known as the "Enhanced composite damage" model, was selected for modelling the failure characteristics. The main parameters of the material card are shown in Figure 6 a), while its behavioral characteristics are shown in Figure 6 b). The material card can change the constitutive properties of the material after reaching certain threshold values and can model the behavior of the material by deleting elements declared as destroyed, causing so-called element death in the system. The MAT54 card utilizes the Chang-Chang failure criterion, described in more detail in the LS-Dyna material model manual [14]. After defining the constitutive, strength, and strain limit parameters and the failure criterion of the material model (Figure 6 a) groups 1, 4, 6, 7, respectively) and its local orientation parameters (Figure 6 a) group 2), the progressive failure parameters were defined and fine-tuned (Figure 6 a) groups 3, 5). The initial values of these were taken from the publication of Feraboli et al. [15] and were tuned in an iterative process to show the closest match with our test curves and with the local deformations obtained with DIC.

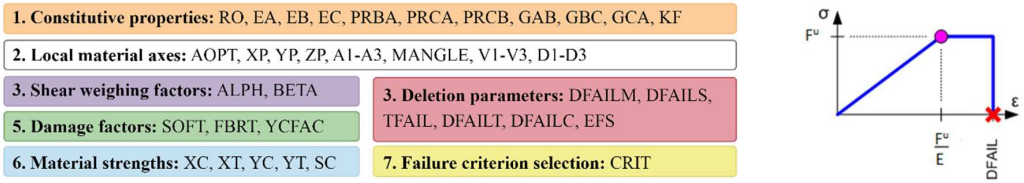

(a) (b)

Figure 6. Table (a) [16] and graph (b) [17] show the behavior of the engineering constants of the MAT54 material card in logical groups. The purple dot indicates the location of ply failure, and the red X indicates the location of element deletion due to element death.

The different sections of the complex curves are dominated by the effects of the different engineering constants, so for example, the moduli can be tuned well from the initial linear section, and information on the sequence and limit values of the different failure modes can be obtained from the local force maxima at failure (Figure 7: numbered local failures). The difficulty of the task is due to the co-occurring effects, which are difficult to separate from each other and which, by their nature, cannot be tuned independently. This can be addressed either by performing several simpler tests separately or by parallel simulation validation on independent, complex problems.

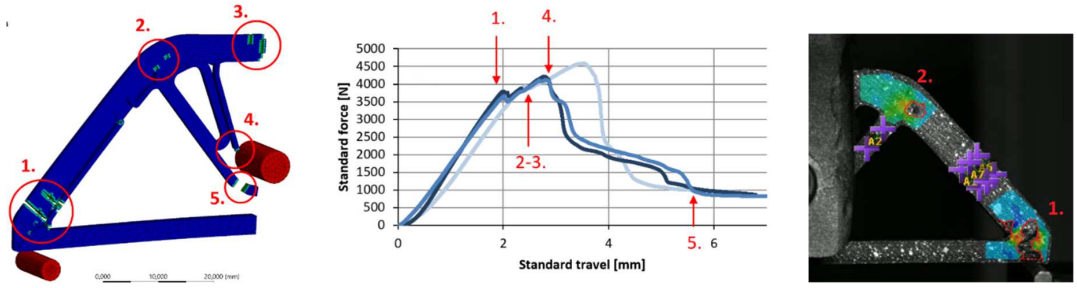

(a) (b) (c)

Figure 7. The location, time, and extent of failure of the elements (a) had to be adjusted based on the curves from the test and the video image of DIC strain measurement (c), in which the adjustment of the non-physical parameters was most challenging.

6. Results and their evaluation

In the fine-tuning of the parameters, the 45th iteration led to the simulation result shown in red in Figure 8, which was considered to be in good agreement with the tests. The abrupt drop in the simulation's reaction force values at 3.2 mm deformation, followed by a "rebound", is attributed to the breaking of the fiber bundles during the load, and the elastic energy release, which is not damped in the simulation, where the matrix material is modelled as linearly elastic. In reality, the PA6-based matrix material is a highly viscoelastic polymer, and its damping effect significantly influences the second, downward half of the failure curve.

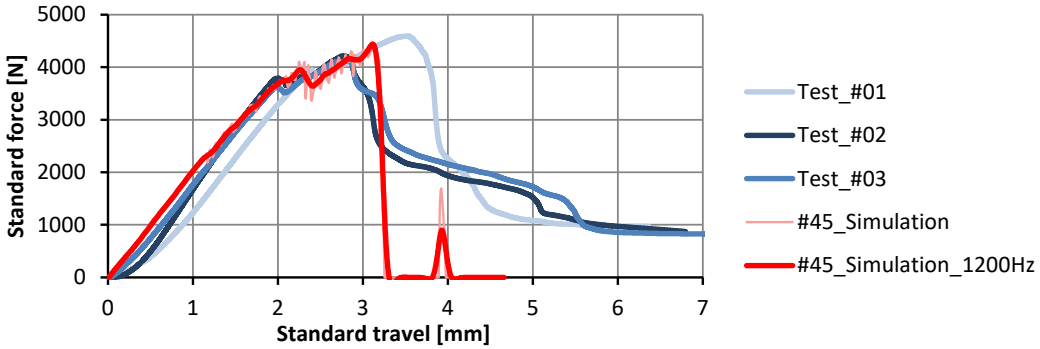

Figure 8. The measured force-deformation curves (blue) and the values of the final simulation (pink), on which a 1200 Hz Butterworth filter was applied (red) to improve the transparency of the values.

The values of the engineering constants for the last simulation can be found in Table 1 (b). The matrix material was modelled with isotropic material properties throughout, with a modulus of 1.4 GPa and a Poisson's ratio of 0.39. All bonded constraints in the final simulation, including delamination phenomena, were set with a maximum normal and shear load of 60 MPa. When this threshold was exceeded, the constraint was removed between the nodes of the respective elements.

Table 1. Material properties of the fiber-reinforced filament used for the initial simulation (a) and the tuned MAT54 material card (b). The constants in grey were unknown in the initial simulation and were determined during the simulation iterations, while the crossed-out parameters were not used in the final simulation.

*MAT_054 (ENHANCED_COMPOSITE_DAMAGE): Mpa, sec, mm, g/cm^3							BASELINE
mid	ro	ea	eb	ec	prba	prca	prcb
0	1,4	70650	1790	1790	0,008112	0,008112	0,41
gab	gbc	gca	kfail	aopt			
700	630	700	0	0			
xp	yp	zp	a1	a2	a3	mangle	
0	0	0	0	0	0	0	
v1	v2	v3	d1	d2	d3	dfailm	dfails
0	0	0	0	0	0	0,246	0,176
tfail	alph	soft	fbrt	ycfac	dfailt	dfailc	efs
0,00E+00	0	0	0	0	0,027	-0,022	0
xc	xt	yc	yt	sc	crit	beta	
-460	930	-36	36	32	0	0	

(a)

*MAT_054 (ENHANCED_COMPOSITE_DAMAGE): Mpa, sec, mm, g/cm^3							FINAL
mid	ro	ea	eb	ec	prba	prca	prcb
1	1,4	64700	1600	1600	0,008112	0,008112	0,41
gab	gbc	gca	kfail	~~aopt~~			
627	570	627	6470	0			
~~xp~~	~~yp~~	~~zp~~	~~a1~~	~~a2~~	~~a3~~	~~mangle~~	
0	0	0	0	0	0	0	
~~v1~~	~~v2~~	~~v3~~	~~d1~~	~~d2~~	~~d3~~	dfailm	~~dfails~~
0	0	0	0	0	0	0,25	0
tfail	alph	soft	fbrt	ycfac	dfailt	dfailc	~~efs~~
5,00E-10	0	0	0,8	3	0,027	-0,02	0
xc	xt	yc	yt	sc	crit	~~beta~~	
-573	860	-38	38	38	54	0	

(b)

7. Discussion

We presented a new method for the finite element modelling of continuous fiber-reinforced composites produced by automated manufacturing. We used the base-coordinate sweep method, coupled with the LS-Dyna explicit environment, and a MAT54 material card tailored for UD composites. The simulations and the validation tests were carried out on a topology-optimized test specimen subjected to three-point loading, which proved to be a good choice due to the complex load states in the specimen. The verification tests were performed with the addition of a DIC system, the results of which were later used to explore the local failure characteristics and finally compared with our simulation results. The constitutive parameters of the material model were partly taken from literature data and partly from our tests and calculations, while the unmeasured constants, which have only mathematical content, were determined in a heuristic, iterative way. The obtained results demonstrate a promising correlation with the measured values, but our investigation shows that the viscoelastic properties of the matrix material cannot be neglected, so their proper modelling requires further work. Overall, the presented method provides a suitable modelling basis for continuous fiber-reinforced composites produced by automated methods, thus greatly improving the engineering applicability of these structural materials produced with novel technology.

Acknowledgments

The project supported by the Doctoral Excellence Fellowship Programme (DCEP) is funded by the National Research Development and Innovation Fund of the Ministry of Culture and Innovation and the Budapest University of Technology and Economics, under a grant agreement with the National Research, Development and Innovation Office.

The research reported in this paper was supported by the National Research, Development, and Innovation Office (NRDI, Hungary) through grants OTKA FK134336 and OTKA K 138472.

Project no. TKP-6-6/PALY-2021 has been implemented with the support provided by the Ministry of Culture and Innovation of Hungary from the National Research, Development, and Innovation Fund, financed under the TKP2021-NVA funding scheme.

Project no. 2022-2.1.1-NL-2022-00012 „National Laboratory for Cooperative Technologies” has been implemented with the support provided by the Ministry of Culture and Innovation of Hungary from the

National Research, Development, and Innovation Fund, financed under the National Laboratories funding scheme.

References

[1] Sigmund O and Maute K 2013 Topology optimization approaches: A comparative review *Struct. Multidiscip. Optim.* **48** 1031–55
[2] Hou Z, Tian X, Zheng Z, Zhang J, Zhe L, Li D, Malakhov A V. and Polilov A N 2020 A constitutive model for 3D printed continuous fiber reinforced composite structures with variable fiber content *Compos. Part B Eng.* **189** Paper ID: 107893
[3] He Q, Wang H, Fu K and Ye L 2020 3D printed continuous CF/PA6 composites: Effect of microscopic voids on mechanical performance *Compos. Sci. Technol.* **191** Paper ID: 108077
[4] Somireddy M, Czekanski A and Atre S V. 2022 Modelling of Failure Behaviour of 3D-Printed Composite Parts *Appl. Sci.* **12** 1–13
[5] Oberlercher H, Heim R, Laux M, Berndt A, Becker C and Amancio- S T 2021 Additive manufacturing of continuous carbon fiber reinforced polyamide 6 : The effect of process parameters on the microstructure and mechanical properties *Procedia Struct. Integr.* **34** 111–20
[6] Chen Y and Ye L 2021 Topological design for 3D-printing of carbon fibre reinforced composite structural parts *Compos. Sci. Technol.* **204** Paper ID: 108644
[7] Szederkényi B 2021 *Újszerű tervezési és gyártási módszer alkalmazhatóságának vizsgálata a Formula Student versenyautó polimer kompozit alkatrészének fejlesztésében* (Master thesis, Budapest University of Technologies and Economics, Department of Mechanical Engineering)
[8] Sauer M 2018 *Evaluation of the Mechanical Properties of 3D Printed Carbon Fiber Composites* (South Dakota State University, Department of Mechanical Engineering)
[9] Zhang H, Chen J and Yang D 2021 Fibre misalignment and breakage in 3D printing of continuous carbon fibre reinforced thermoplastic composites *Addit. Manuf.* **38** Paper ID: 101775
[10] Goh G D, Toh W, Yap Y L, Ng T Y and Yeong W Y 2021 Additively manufactured continuous carbon fiber-reinforced thermoplastic for topology optimized unmanned aerial vehicle structures *Compos. Part B Eng.* **216** Paper ID: 108840
[11] Blok L G, Longana M L, Yu H and Woods B K S 2018 An investigation into 3D printing of fibre reinforced thermoplastic composites *Addit. Manuf.* **22** 176–86
[12] Markforged Material Datasheet Composites
[13] Ghebretinsae F 2019 *Mechanical testing and finite element analysis Of 3D printed continuous carbon fiber reinforced Onyx® thermoplastic* (Master thesis, Universitetet i Stavanger, Department of Engineering Structures and Materials Science,)
[14] LS-Dyna LS-DYNA Manual: Volume II R13
[15] Feraboli P, Wade B, Deleo F, Rassaian M, Higgins M and Byar A 2011 LS-DYNA MAT54 modeling of the axial crushing of a composite tape sinusoidal specimen *Compos. Part A Appl. Sci. Manuf.* **42** 1809–25
[16] Wade B, Feraboli P, Osborne M and Rassaian M 2015 *Simulating Laminated Composite Materials Using LS-DYNA Material Model MAT54 : Single-Element Investigation* (Seattle)
[17] Wade B, Feraboli P and Osborne M 2015 *Simulating Laminated Composites Using LS-DYNA Material Model MAT54 Part I : [0] and [90] Ply Single-Element Investigation* (Seattle)